

Variational Quantum Brush: Adding Optimization to Arts

Luminists team: Ali Abbassi, Henrique Ennes, Chih-Kang Huang
Jui-Ting Lu, Massinissa Zenia
Mentor: Astryd Park (MOTH Quantum)

Abstract

This report formalizes two new mechanisms for MOTH Quantum’s *Quantum Brush* project [17], *Steerable* and *Chemical*. Both brushes are inspired by the important family of variational quantum algorithms and translate quantum computational processes into visual parameters. Nevertheless, they serve very different artistic and implementation purposes. *Steerable* utilizes geometric control theory to translate the colors from one canvas to another. This is possible through the use of neural networks for the estimation of a smooth trajectory from the source to the target. By picking the trajectory’s parameter, the user can decide the degree of change applied to the source. *Chemical*, on the other hand, uses intermediate steps of the VQE algorithm from quantum chemistry to locally change the colors of the canvas. In this sense, the brush encodes not only the physical process related to the ground state of molecules but also the behavior of the variational algorithm itself. This document introduces the precise mathematical definitions and motivations of the variational brushes, describes their implementations—which are available at <https://github.com/mothorchids/QuantumBrush>—and showcases early artistic experiments. We also outline future directions for improving the new brushes and the user’s experience with them.



Figure 1: Steerable effect applied to Renoir’s *Bal du moulin de la Galette* using a red parrot as target image.

1 Introduction

Variational quantum algorithms (*VQAs*) encompass some of the most anticipated techniques of real quantum advantage. These methods are designed to leverage both classical and quantum paradigms to minimize an objective function that is evaluated on quantum states. In practice, this is possible through the iterative application of a parametric family of quantum circuits, whose optimal parameters are approximated by classical continuous optimization algorithms. However, because quantum spaces can be used to encode exponentially more information than classical bits, this often leads to the efficient solution of problems that are expected to be hard to tackle by other techniques. Applications of VQAs already abound, ranging from the original variational quantum eigensolver (*VQE*) used in quantum chemistry [31], to portfolio optimization tasks [1]. Particularly interesting to us is their use in the arts, mainly in quantum music [23, 29]. Since VQAs belong to the very restricted classes of algorithms known to be noisy intermediate-scale quantum (*NISQ*) [3], they also figure as good candidates for implementation as quantum brushes [17].

In this report, we describe two new brushes: *Steerable* and *Chemical*. Although both are based on variational methods, their construction and artistic aims are significantly different. *Steerable* uses concepts of geometric control theory to merge two pieces of art, represented as distinct quantum states. Geometric control theory can be understood as the study of how systems governed by physical laws evolve when their motion can be influenced by certain controllable degrees of freedom. It tells us, for example, that a car can park in parallel, even though it cannot move directly sideways. For us, control theory will be used in its quantum incarnation to smoothly drive a region of an input canvas into another. This can be visualized as a *path* of canvases whose beginning is full of pieces very similar to the original image but that start to look more and more like the target as one gets to its end. The user, by controlling a continuous parameter, decides where to stop on this road.

The idea behind *Chemical*, on the other hand, is to use the minimization procedure of *variational quantum eigensolvers* (*VQE*) to generate a parametric family of quantum circuits $U(\boldsymbol{\eta})$ such that, at the convergence limit to optimal parameters $\boldsymbol{\eta}^*$, $U(\boldsymbol{\eta}^*)$ applied to some fixed state $|\Psi_{\text{HF}}\rangle$ (see Section 3.1 for details) represents the ground state of a molecule. This means that while the variational parameters change throughout the optimization, the *physical process* given by $U(\boldsymbol{\eta})$ gets closer and closer to the evolution of $|\Psi_{\text{HF}}\rangle$ towards the minimal energy configuration of the molecule. By applying these circuits to the angular encoding of different pixels in a finite stroke, we define a path of states whose final points evolve like a molecular system, but whose intermediate values “record” the steps of the variational algorithm. Therefore, not only will the brush be driven by a real-life chemical process but also by the algorithmic tool used in current quantum research to *study* that same process. In a sense, it is an attempt to bring cutting-edge scientific evolution to the artists’ fingertips.

This report is divided according to these two brushes, starting with *Steerable* (Section 2) and then moving to *Chemical* (Section 3). In each of these sections, we give a general explanation of their artistic features, after which we describe their mathematical formulation and implementation¹ in further detail. Due to time constraints, we were unable

¹The code is fully available online.

Application of the brush: <https://github.com/mothorchids/QuantumBrush>;
Background of implementation: <https://github.com/mothorchids/Luminists-Quantum-Brushes>.

to present an in-depth introduction to the theoretical background behind the brushes' concepts, but we hope that the interested reader can profit from the cited bibliography and the expanded information of the Appendix A. Conclusions and directions for future improvements are described in Section 4.

2 Steerable

In quantum mechanics, control theory is typically concerned with manipulating the behavior of quantum systems, such as atoms, molecules, or qubits, using precisely shaped external fields like lasers, microwaves, or magnetic pulses. By fine-tuning these controls, scientists can steer a system's evolution toward a desired quantum state or outcome. For example, laser pulses can be optimized to drive chemical reactions along specific pathways, or microwave signals can be used to perform accurate qubit rotations in a quantum computer. Through such techniques, quantum control² enables both fundamental discoveries in physics and practical advances in quantum technologies [6, 14, 18].

Steerable applies this framework to drive one artwork into another. Notice that, despite intent similar to the Collage brush already implemented [17], *Steerable* is mechanically very different. Instead of attempting to copy the state $|p_0\rangle$ of the source work, *Steerable* looks for a parametrized family of quantum circuits $U(t)$ such that, when $t = 0$, it does not change $|p_0\rangle$, but, when $t = 1$, it reaches a state very close to $|p_1\rangle$, the state of the target canvas. This means that for values of t in between 0 and 1, $U(t)|p_0\rangle$ will represent a canvas "in between" the original and the target, although *not* a mixture of both—or, at least, not in the classical sense of the word. Quantum control, therefore, opens an entirely new creative frontier. Through controlled quantum dynamics, one can generate visual and interactive art that reflects the inherent beauty and unpredictability of quantum mechanics, translating the invisible behaviors of the quantum world into tangible aesthetic experiences.

2.1 Theoretical framework

Let us suppose that the two canvases have been discretized into pixel grids and that \mathcal{C}_1 and \mathcal{C}_2 are lasso-defined copy and target regions. We can further assume that \mathcal{C}_1 and \mathcal{C}_2 are represented by quantum states, respectively denoted $|p_0\rangle$ and $|p_1\rangle$. We aim to steer $|p_0\rangle$ to $|p_1\rangle$ using quantum circuits representing *drifts* and *controls* with the least energy possible. For such a purpose, we take a *bilinear multilevel* quantum system model [2] and consider the following time-optimal control problem

$$\min_{(*)} \left(1 - F(|\rho(1)\rangle, |p_1\rangle) + \int_0^1 |u|^2(\eta, s), ds \right) \quad (1)$$

subject to

$$\left\{ \frac{d}{dt}|\rho(t)\rangle = -iH(t)|\rho(t)\rangle, \ |\rho(0)\rangle = |p_0\rangle, \right. \quad (2)$$

where $F(|\rho(1)\rangle, |p_1\rangle)$ is the quantum fidelity between $|\rho(1)\rangle$ and $|p_1\rangle$ and $H(t)$ is the Hamiltonian defined by

$$H(t) = H_0 + u_1(t)H_1 + \dots + u_m(t)H_m, \quad (3)$$

²For an overview of quantum control theory, including its mathematical background, refer to [14].

where we call H_0 the *drift* Hamiltonian, H_1, \dots, H_m the *control* Hamiltonians, and the real functions $u_1(t), \dots, u_m(t)$ the *control amplitudes*. Due to the time dependence of the Hamiltonian, it is in general difficult to obtain analytical solutions to (2), making the problem non-trivial.

We are here interested in finding appropriate controls u_1, \dots, u_m to steer $|p_0\rangle$ to $|p_1\rangle$, that is, whether there exist $u_1, \dots, u_m \in L^2([0, 1])$ such that the solution $|\rho(t)\rangle$ to (2) satisfies $|\rho(1)\rangle = |p_1\rangle$. We say that the system (2) is *exactly controllable* if it is always possible to steer any quantum state to any other state.

Exact controllability of (2) has been first investigated in [33] and has been characterized in [2] in terms of the Lie algebra³ generated by the Hamiltonians iH_0, iH_1, \dots, iH_m . Namely, we have

Theorem 2.1. [2] *The system (2) is exactly controllable if and only if the Lie algebra generated by $\{iH_0, iH_1, \dots, iH_m\}$ satisfies*

$$\text{Lie}\{iH_0, iH_1, \dots, iH_m\} = \mathfrak{su}(N), \quad (4)$$

with $N = 2^n$ where n is the number of qubits.

It should be noted that the exact controllability of the system (2) can be achieved with a drift Hamiltonian H_0 , and only one control Hamiltonian H_1 , see [27, 37]. However, such Hamiltonians consist of large sums of Pauli operators, which makes them impractical from a quantum control perspective, and the resulting control amplitude u tends to be less smooth, making its numerical determination challenging⁴.

In this work, we consider a bilinear system where the number of control Hamiltonians, m , matches the number of qubits, n . This hypothesis remains reasonable since the state space dimension scales exponentially, whereas the number of controls scales linearly. The dimensions of the state space and the associated Lie algebra for 2 to 4 qubits are listed in Table 1.

Qubits	Control dim. (m)	State space dim.	dim($\mathfrak{su}(N)$)
2	2	6	15
3	3	14	63
4	4	30	255

Table 1: Dimensions for different qubit numbers.

Once the appropriate Hamiltonians are chosen, the remaining challenge is to determine explicit controls u_1, \dots, u_n capable of steering $|p_0\rangle$ to the target state $|p_1\rangle$. Several algorithms have been proposed, such as GRAPE [25] and CRAB [8]. Here, we opt to approximate the controls using neural networks, which, to the best of our knowledge, remain a relatively unexplored option. However, neural networks offer a powerful analytical framework for studying properties such as stability in architecture design, see for example [9].

Explicitly, we train a neural network to approximate $u(\boldsymbol{\eta}, t)$ by minimizing (1) and optimizing the parameters $\boldsymbol{\eta}$ through backpropagation. To evaluate $|\rho(1)\rangle$ in (1), we first

³For a gentle introduction to Lie algebras, refer to [15, 22, 26].

⁴Exact controllability with a more natural set of Hamiltonians, such as tensor products of Pauli operators (Pauli strings), has been investigated in [12, 35].

note that

$$\begin{aligned} |\rho(1)\rangle &= U(1)|\rho(0)\rangle \\ &= \exp\left(-i \int_0^1 H(s) ds\right)|\rho(0)\rangle. \end{aligned}$$

One can express a parametric family of circuits for $U(1)$ by approximating the time-ordered exponential using a second-order splitting scheme

$$\begin{aligned} U(1) \approx \prod_{k=1}^N &\left(\exp\left(-iH_0 \frac{\Delta t}{2}\right) \exp\left(-iu(k\Delta t)H_1 \frac{\Delta t}{2}\right) \dots \exp\left(-iu(k\Delta t)H_n \frac{\Delta t}{2}\right) \right. \\ &\left. \exp\left(-iu(k\Delta t)H_n \frac{\Delta t}{2}\right) \dots \exp\left(-iu(k\Delta t)H_1 \frac{\Delta t}{2}\right) \exp\left(-iH_0 \frac{\Delta t}{2}\right) \right) \end{aligned} \quad (5)$$

with N the number of discrete timesteps within the interval $[0, 1]$ and $\Delta t = 1/N$. Although complicated, the circuits described by (5) can be efficiently implemented as strings of Pauli gates, making the preparation of $|\rho(t)\rangle$ feasible.

In our test case, training is usually fast and achievable with shallow neural networks; however, we note that faster but less accurate approximations are possible through early stopping. Furthermore, this training approach is unsupervised and not data-driven, unlike most machine-learning applications.

Once $u(\eta, t)$ is estimated, $|\rho(t)\rangle$ can be evaluated for any $t > 0$ as in (5). That is, while the constraints sets $|\rho(0)\rangle = |p_0\rangle$ and, for good solutions, $|\rho(1)\rangle$ is close $|p_1\rangle$, nothing prevents us from considering states $|\rho(t)\rangle$ for $t > 1$. This means that, instead of using Steerable only to interpolate between $|p_0\rangle$ and $|p_1\rangle$, we can also use it to *extrapolate* to states beyond the target. Using the analogy of a path of canvases, this can be seen as extending the road beyond its final stop, while still retaining its geometric information. For this reason, we allow the value of t , the main user-controlled parameter, to range from 0 to 1, or even beyond 1 in the case of extrapolation.

It should be noted that, despite being hybrid and involving a minimization problem, the quantum control technique described here deviates significantly from the usual VQA approach. Nevertheless, it bears enough similarities to belong among what we classify as variational brushes, that is, the brushes inspired by variational methods.

2.2 Implementation

The implementation of the steerable brush is summarized in the diagram in Figure 2, which illustrates the flow of information throughout the system.

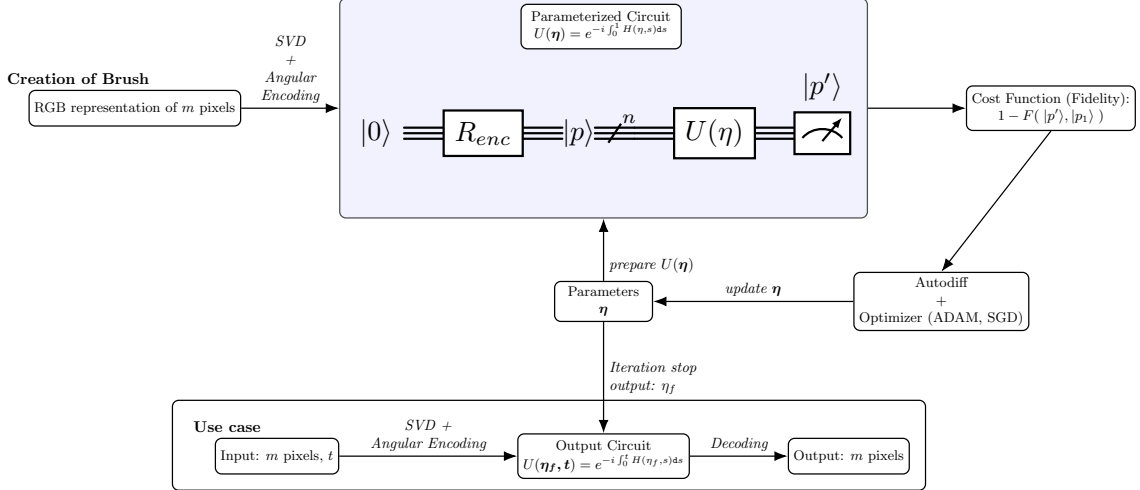


Figure 2: Diagram summarizes the learning process behind Steerable.

We start by describing the user-defined parameters. The user marks three regions—source, target, and paste—by directly sketching them on the canvas. The paste region may also be specified as a single point (i.e., two circles and one point), in which case the steered source image is pasted into the region whose barycenter corresponds to that point. By default, "`Source = Paste`" is *false*; it should be enabled only when no separate paste region is defined.

A model is then trained to compute a quantum circuit that transforms the source region into the target region. After training, the learned transformation is applied to the paste region (which may be identical to the source). The main parameter is t , which controls how far along the learned transformation the system evolves:

- $t = 0 \rightarrow$ source-like,
- $t = 1 \rightarrow$ target-like,
- $t > 1 \rightarrow$ extrapolation beyond the target (may produce novel effects).

Additional parameters include:

- **timestep**: number of discrete steps used to approximate the circuit's evolution. It also controls the degree of transition smoothness in the brush dynamics. Its default value is 25.
- **controls**: number of features used to represent a patch—equivalently, number of qubits.
- "`Source = Paste`": forces the paste region to coincide with the source region.

Optional visualization controls include "`show source & target`" (along with boundary settings "`show color`" and "`show thickness`"), which display the reference regions with boundaries rendered in the selected color and thickness.

Given a source state and a target state, our goal is to construct a parameterized quantum circuit that acts through controlled Hamiltonian dynamics to steer the source towards the target. In that, we follow these steps:

1. For $n \in \{2, 3, 4\}$, we set

$$\begin{cases} H_0 &= \sum_{k=1}^{n-1} X_k X_{k+1} + Y_k Y_{k+1} + Z_k Z_{k+1} \text{ and} \\ H_k &= \begin{cases} X_k & \text{if } k \equiv 1 \pmod{3}, \\ Y_k & \text{if } k \equiv 2 \pmod{3}, \\ Z_k & \text{if } k \equiv 0 \pmod{3}, \end{cases} \quad \text{for } 1 \leq k \leq n. \end{cases} \quad (6)$$

One can check that the exact controllability condition (4) is verified.

2. Let $|p_0\rangle$ and $|p_1\rangle$ be the color encodings of two selected regions of the canvas. Details on the color encoding are provided at the end of the section. We consider the time optimal control problem defined in equations (1) and (2).

Due to the choice of Hamiltonians in (6), the parametrized quantum circuit $U(1)$ defined in (5) can be written as a sequence of rotation gates R_X, R_Y, R_Z , which provides standard quantum utilities. Namely, we have

$$U(1) \approx \prod_{k=1}^N \left(\exp\left(-iH_0 \frac{\Delta t}{2}\right) R_{X_1} \left(-u(k\Delta t) \frac{\Delta t}{4}\right) R_{Y_2} \left(-u(k\Delta t) \frac{\Delta t}{4}\right) \dots \right. \\ \left. R_{Y_2} \left(-u(k\Delta t) \frac{\Delta t}{4}\right) R_{X_1} \left(-u(k\Delta t) \frac{\Delta t}{4}\right) \exp\left(-iH_0 \frac{\Delta t}{2}\right) \right) \quad (7)$$

where N is a user-defined smoothness parameter, with default value 25, and $\Delta t = 1/N$.

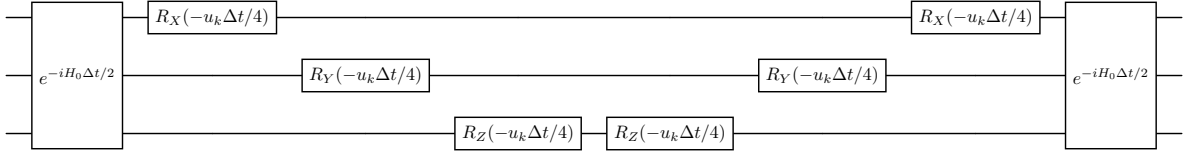


Figure 3: The k th part of the splitting circuit (7) for 3 qubits

3. We train the neural network $u(\eta, t)$ by minimizing (1). Forward evaluation is done using (7) in PennyLane, and we backpropagate gradients through the neural network using JAX.

Once training is complete, we evaluate $|\rho(t)\rangle$ in the same way as in step 2 for the user-defined time $t > 0$, and then paste the resulting state into the target region. A simulated trajectory that illustrates the steering of one state to another in the 2-qubit state space is shown in Figures 4 and 5. Due to the constraints imposed by the Hamiltonian, the trajectory is not geodesic in the quantum space. Still, it can steer the initial to the target state when $t = 1$.

Finally, we elaborate on how we obtain source and target states from selected regions. Encoding every pixel into a qubit can become computationally expensive for high-resolution images. Inspired by the Collage brush, we reduce the color information using Singular Value Decomposition (SVD).

Specifically, let $C \in \mathcal{M}_{m \times d}$ be the matrix encoding ($d = 3$ for RGB and $d = 4$ for RGBA) of m pixels. Its SVD is given by

$$C = USV,$$

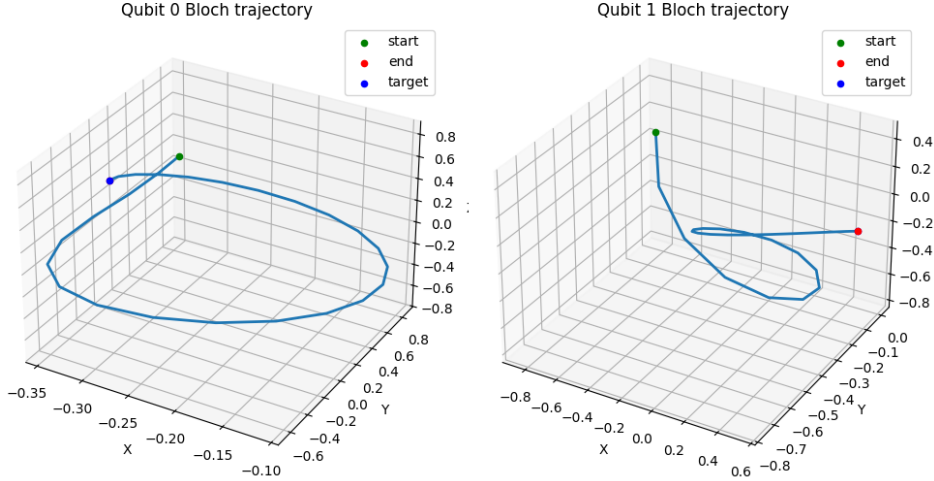


Figure 4: Visualization of the steering effect for 2 qubits.

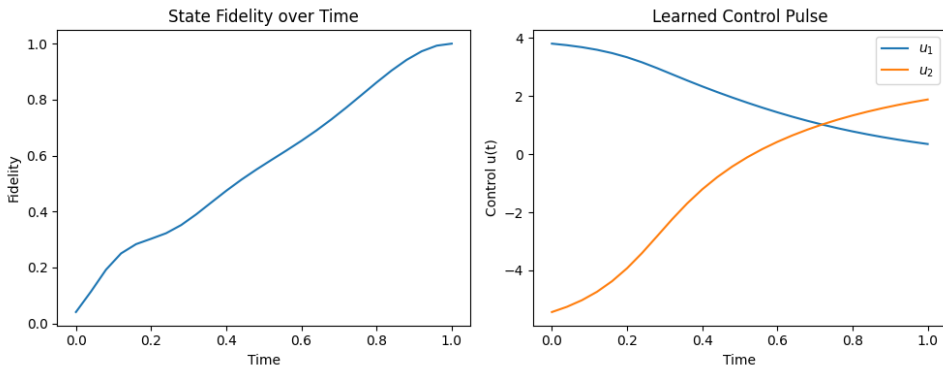


Figure 5: Fidelity evolution over time and the control amplitudes u_1 and u_2 .

where $U \in \mathcal{M}_{m \times d}$ is semi-unitary, $S \in \mathcal{M}_{d \times d}$ is diagonal with strictly positive entries, and $V \in \mathcal{M}_{d \times d}$ is unitary. We note that, while Collage uses RGB encoding [17], we use RGBA, where the extra ‘‘A’’ is a parameter for transparency (often denoted alpha in computer vision).

In our implementation, we provide the following three options:

- 2 qubits: We use the logarithm of the 4 values on the diagonal of S . We note it as $\hat{S} = \log(S) = \{\log(s_i) | s_i \in \text{diag}(S)\}$;
- 3 qubits: We consider 4 values of \hat{S} and 4 additional values from $V\hat{S}$;
- 4 qubits: use the 16 coefficients from four vectors of \hat{S} , $V\hat{S}$, $V^2\hat{S}$ and $V^3\hat{S}$.

For every number of qubits n , we construct the encoding as

$$\text{state} = \begin{pmatrix} \text{Id}_d & O & O & O \\ O & V & O & O \\ O & O & \ddots & O \\ O & \dots & \dots & V^{2^n-2-1} \end{pmatrix} \begin{pmatrix} S \\ S \\ \vdots \\ S \end{pmatrix} \text{ where } \hat{S} = \log(S).$$

In the evaluation stage, the output state has the same length as the input (either the source or a newly defined paste region). We recover these states as coefficients in the



Figure 6: Target for the application of the Steerable brush for generating Figure 1.

matrices S and V , taking care to account for the normalization factors. Note that the reconstructed pixels obtained by multiplying the new matrices U , S , and V may contain negative values or exceed 255. We simply clip the results to the valid range $[0, 255]$.

2.3 Outcome

Figure 1 shows the result of applying the Steerable effect with target Figure 6, taking Renoir’s *Bal du moulin de la Galette* [34]. There, we show equally spaced values of t ranging from 0 to 1. As t increases, the initially smooth blend of colors, characteristic of Renoir’s work, diverges toward the vivid colors of the parrot colors. Interestingly, however, when t approaches 1, the colors seem to decay towards a gray spectrum. This pattern seems to be frequent in several of our extrapolation experiments, although not in all. We are still unsure of the causes of this gray decay, but some hypotheses are discussed in Section 4. Note that the convergence to a different color palette at $t = 1$ is not unexpected: perfect convergence to the target would only happen in the perfect scenario in which the final fidelity in equation (1) is maximized. Unfortunately, for practical training, this will hardly be the case, meaning that the expected convergence to the target colors at the $t = 1$ limit will likely only be approximated. Adding more controllability or experimenting with different approximation algorithms and color encoding might bring the state when $t = 1$ closer to the target.

Figure 7 shows the application of Steerable with **controls** equal to 2 on two images of Andy Warhol’s *Marilyn Diptych* silk screen series [39]. The first two rows indicate applications of Steerable for t that vary uniformly from 0 to 1, where the target is the leftmost image of the third row. Similarly, the last two rows indicate applications of steerable targeting the leftmost image of the first row. Note that while the use of Steerable

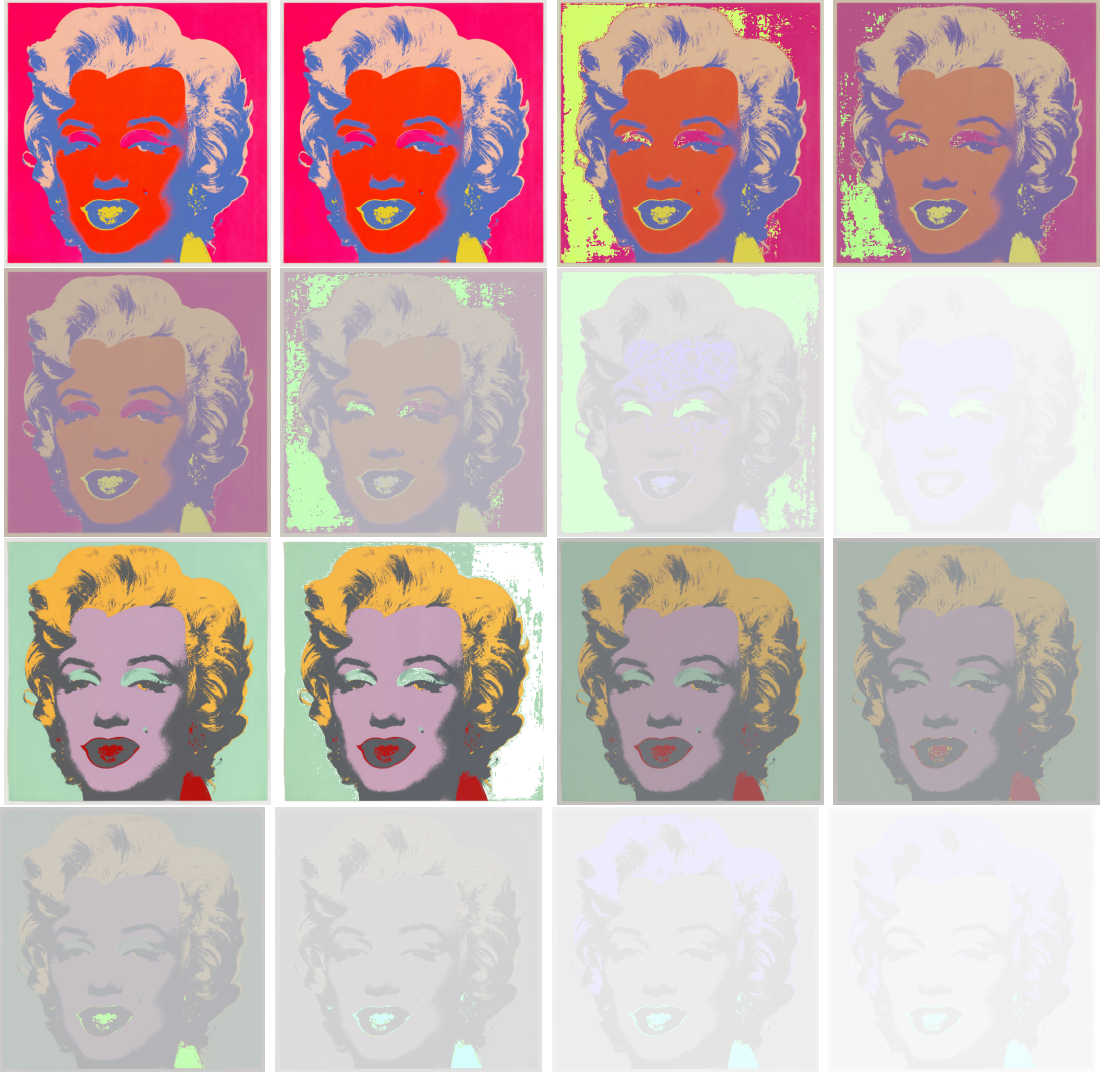


Figure 7: Steerable effect applied to Warhol’s *Marilyn Diptych*. The leftmost images of the first and third rows were used as the source and target.

depicted on the first two rows drifts the very reddish colors of the source to the correct green and blue directions, it fails to converge the colors of the second source towards red in the last couple of rows. Moreover, in both cases, the aforementioned convergence towards gray can also be observed. In our experiments with Warhol’s work, we have noticed that this tendency towards gray is significantly mitigated by introducing more control; however, the colors for mid-range values of t start blending rapidly, which directly jeopardizes visualization. We believe that this tension between grayness and too much noise might be related to the usual under- and overfitting in machine learning—which, on its own, is related to the bias-variance issue of statistics [4]—but, once more, further investigation is required.

Finally, Figure 8 shows an application of the steerable brush in Joan Miró’s *El Jardín* [30]. In particular, we select the white bird as the source and steer it into two additional bird shapes using 2 (top) and 3 (bottom) controls. The star in the top-left corner is likewise steered into two copies using 3 controls (middle) and 4 controls (bottom left). The parameter t was set to values in between 0.2 and 0.4. We also paste several other small elements, which we leave to the reader as a playful exercise of “Where’s Charlie?”.



(a) Original *El Jardín* by Joan Miró.



(b) Application of Steerable to Miró's piece.

Figure 8

3 Chemical

In its century of existence, quantum mechanics has been responsible for several technological and scientific revolutions. Still, few were as groundbreaking as the description of the periodic table through Pauli’s exclusion principle. The scientific understanding that atomic particles behave differently from the old Newtonian rules of physics forever entangled the fields of quantum mechanics and chemistry, making the study of the former a foremost ingredient in the latter. For instance, quantum mechanical considerations imply that molecules—amalgamations of atoms sharing electrons—are only allowed to be found within some discretely separated energetic states. Being a little more explicit here, a hydrogen molecule, H_2 , for example, is associated with a whole tower of energy levels E_0, E_1, E_2, \dots that it can have, but it can never be found with energy equal to a value between two of these numbers. In other words, molecular energy is *quantized*. For the most part, molecules are found in the minimum energy state possible E_0 , their *ground state*, although sometimes they will be seen in higher states called *excitations*. As it turns out, finding the ground states of molecules is an extremely complicated computational problem, and techniques based on quantum computers have become competitive candidates to deal with it.

VQE is one of these techniques. It expresses the energy of a molecule (or, to be precise, of its expectation value) as an objective function in an optimization program, and, at each step, it searches for circuits that minimize this quantity, which is equivalent to saying that it searches for the molecule’s ground state energy. When it works well—which unfortunately is not the case for every single molecule—VQE finds not only E_0 , but also a last outputted circuit that transforms a reference state into the molecule’s ground state.

Chemical serves as a visualization of VQE. It uses the algorithm’s parametric circuits

to drive changes at each pixel crossed by the stroke. Once more, when the algorithm correctly converges, its last transformation corresponds to the evolution of a molecule towards the ground state. In this sense, the brush encodes not only the well-known VQE algorithm, highlighting the most modern advances of quantum research, but also incorporates Nature into the process.

3.1 Theoretical framework

In the VQE formulation of variational algorithms, we suppose that H is a Hermitian (self-adjoint) operator corresponding to the solution of Schrödinger's equations for some molecule⁵. The exact value of H depends not only on the type of molecule, but also on some physical constants such as Planck's and the average distance between the atoms in the molecule (also known as the molecule's *bond distance*). By the Spectral Theorem [20], H can be written as

$$H = \sum_{k=0}^{d-1} E_k |\phi_k\rangle\langle\phi_k|.$$

The eigenstates $\{|\phi_k\rangle\}_{k=0}^{d-1}$ represent the allowed configurations of the electrons in the molecule, while the quantities E_k are the associated energies. In particular, we may always assume $E_0 \leq E_1 \leq \dots \leq E_{d-1}$, in which case the minimum energy allowed, E_0 , is the ground state of the molecule.

The variational principle implies that, given any other state $|\psi\rangle$ (not necessarily equal to one of the eigenstates $|\phi_k\rangle$, but potentially a linear combination of those), the quantity $\langle\psi|H|\psi\rangle$ is at least as big as E_0 , with equality if and only if $|\psi\rangle$ is proportional to $|\phi_0\rangle$. Therefore, the problem of minimizing the quantity $\langle\psi|H|\psi\rangle$ is fully equivalent to finding the ground state of H , up to a proportionality factor. In practice, we look for a state $|\psi\rangle \neq 0$ such that

$$E^* = \min R(\psi) \geq E_0 \quad (8)$$

where

$$R(\psi) = \frac{\langle\psi|H|\psi\rangle}{\langle\psi|\psi\rangle}$$

is known as the *Rayleigh-Ritz* quotient.

The optimization program for equation (8) is the part usually tackled by VQE. This is possible by mapping the fermionic states of the molecule's electrons into the qubits of a quantum circuit and the Hamiltonian into a linear combination of Pauli gates. Refer to Appendix A for details on this and the whole quantum chemistry treatment of this section. We point out that this map depends on the choice of a basis as a hyperparameter; for all experiments, we choose the basis to be STO-3G. Then, a parametrized family of circuits $U(\boldsymbol{\eta})$ is applied to a reference state $|\Phi_{\text{HF}}\rangle$ —called the Hartree-Fock reference state—and the values of $\boldsymbol{\eta}$ are adjusted according to some classical continuous optimization routine—such as line-search or fixed-step gradient descent—to minimize

$$E(\boldsymbol{\eta}) = \langle\psi(\boldsymbol{\eta})|H|\psi(\boldsymbol{\eta})\rangle,$$

where

$$|\psi(\boldsymbol{\eta})\rangle = U(\boldsymbol{\eta})|\Phi_{\text{HF}}\rangle.$$

⁵Hands-on introductions and review of VQE can be found in [16, 32].

The exact form of the parametric circuits $U(\boldsymbol{\eta})$ corresponds to the ansatze of the solution and can be taken to better correspond to the chemical system or to guarantee the efficiency of the hardware. In Appendix A, two of the most popular ansatze are described explicitly. Since we are mainly interested in the simulation of quantum circuits, we opt for the more chemically motivated disentangled unitary coupled cluster ansatz (DUCC). However, the choice of DUCC as an ansatz introduces a second hyperparameter in the form of the ordering of the unitary operators, which, in general, do not commute. Different orderings may lead to different convergence trajectories to the ground state and, consequently, to different parameters for the circuits. Here, we take the standard ordering of operators (again, refer to the Appendix A for details), although we stress that different choices, including usually faster converging ones, are possible.

In each optimization step i in which $\boldsymbol{\eta}_i$ is updated, there will be associated $f_i = f(|\psi(\boldsymbol{\eta}_i)\rangle)$ and $U_i = U(\boldsymbol{\eta}_i)$. In particular, provided that there is good convergence to E^* , we might assume that $\{f_i\}_{i=1}^N$ is an overall decreasing sequence and that $\{U_i\}_{i=1}^N$ gets closer and closer to the process that maps the reference state to the minimizer in equation (8)—i.e., $|\psi(\boldsymbol{\eta}^*)\rangle$ becomes a good approximation of the ground state. The parametric list of circuits $U(\boldsymbol{\eta}_i)$ is the main quantum ingredient in the brush implementation.

3.2 Implementation

The user begins by drawing one or more strokes of some fixed radius on the canvas. As in Aquarela and Smudge, the strokes define arrays of pixels, whose hue and luminosity values (HL) are aggregated by averaging the angular HL of neighboring pixels. Like these other brushes, each of these aggregated HL values $\{(\phi_j, \theta_j)\}_{j=1}^N$ is encoded as qubits through applications of $R_Z(\phi_j)$ and $R_Y(\theta_j)$ gates (see Figure 9). The number of qubits N is chosen to match the total number of pixels in the whole estimated parametric family $\{U(\boldsymbol{\eta}_i)\}_{i=1}^M$; recall that each circuit of the family admits the same number of qubits n_{qub} , meaning $N = M \times n_{qub}$. In our choices of hyperparameters, for example, n_{qub} of the H_2 molecule equals 4. For simplicity, we follow [17] and denote the thus encoded states by $|(\theta_j, \phi_j)\rangle$.

Next, $U(\boldsymbol{\eta}_i)$ is applied to each $|(\theta_j, \phi_j)\rangle$, ultimately changing the encoded states according to the VQE algorithm. The new HL values are reconstructed from the trigonometric transformations of the expectations of the Pauli operators, as described in the appendix of [17]. Once again, assuming convergence, the qubits at the end of the stroke will be mapped to the state $U(\boldsymbol{\eta}^*) \cdot \bigotimes_{j=N-n_{qub}}^N |(\phi_j, \theta_j)\rangle$, where $U(\boldsymbol{\eta}^*)$ is a good approximation of the operator that maps $|\Phi_{HF}\rangle$ to the ground states. Of course, $|\Phi_{HF}\rangle$ is likely very different from $\bigotimes_{j=N-n_{qub}}^N |(\phi_j, \theta_j)\rangle$ and, consequently, $U(\boldsymbol{\eta}^*) \cdot \bigotimes_{j=N-n_{qub}}^N |(\phi_j, \theta_j)\rangle$ will not represent the molecule's minimum energy state. This is where the beauty of Schrödinger's equation lies: $U(\boldsymbol{\eta}^*)$ is an approximation of the *physical process* that takes the Hartree-Fock state to the ground, but this same process can also be applied to any initial quantum state, including an encoding of HL values. In a sense, we are not interested here in the output of the VQE algorithm, but rather in the output process of the algorithm.

As in the other brushes, the user of Chemical has access to a continuous parameter, which here defines the bond distance used by the VQE. However, unlike the other cases, setting the bond distance to a specifically low or high value does not have a direct interpretation in terms of the expected effect, and we invite the user to play with different configurations. Another parameter set by the user is the Number of Repetitions, which varies from 0 to 100 and controls the number of times that the circuits in the parametrized family are repeatedly applied to neighboring qubits. Its object is to make

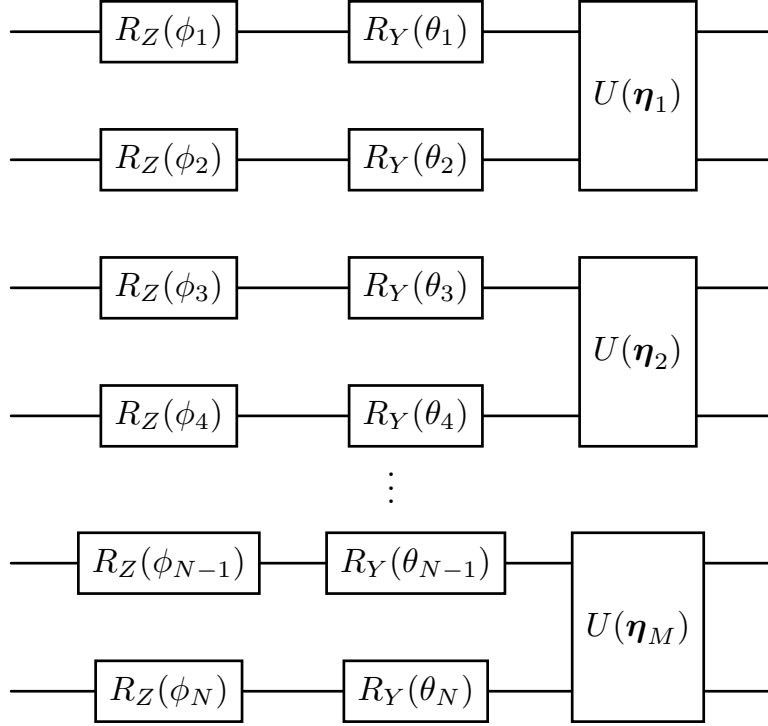
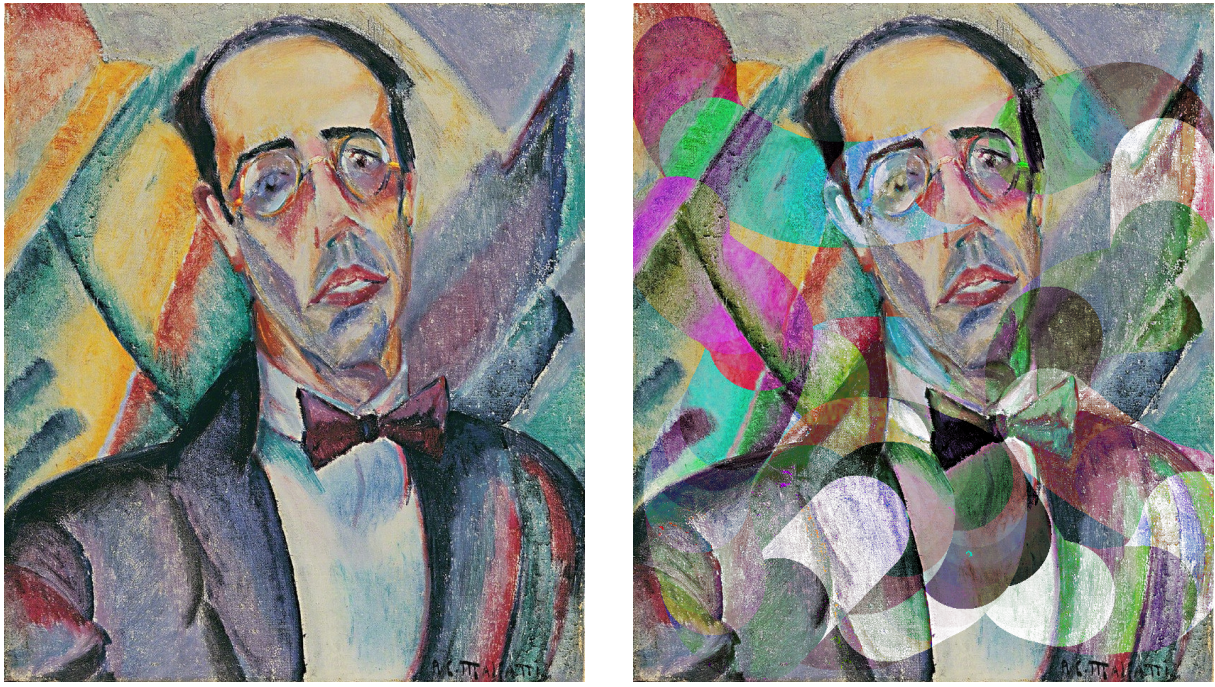


Figure 9: Basic circuit of Chemical. Measurements are not shown. Note that here, n_{qub} equals 2.

the transition between different circuit applications smoother, which is particularly significant for monochromatic pieces. Finally, the stroke’s radius is the last parameter that is adjusted by the user; as usual, it defines the thickness of the stroke.

Two subtleties about Chemical’s implementation should be highlighted here. First, as of now, H_2 is the only molecule available. This is due to the simplicity of the VQE algorithm when applied to it. For the hyperparameters we chose, VQE converges pretty fast to the ground state of H_2 , which can be understood as a manageable number of circuits M . For other molecules, these hyperparameters lead to very slow convergences, which implies values of M some orders of magnitude above the number of qubits created by a usual stroke. Therefore, implementing Chemical for more molecules would require fine-tuning of the hyperparameters, which is an area of research of its own.

Second, instead of running VQE on the user’s machine at each application of the brush, we preprocessed the parametrized families $\{U(\eta_i)\}_{i=1}^M$ at different distance values, which we save as JSON files in a data folder. Although VQE tends to be fast for H_2 , we believe that taking the bulk of the computation off the user’s end improves the experience. Nevertheless, this restricts the applications of Chemical by making it so that only a finite, despite large, set of bond distances can be used in practice. We precomputed VQE families for 1000 bond distances, varying uniformly in the interval from 0.725 to 2.5 Å. The user can choose any floating-point number within this range, but when applying the effect, their choice is projected onto the closest distance for which circuits were precomputed. We are currently working on an implementation that allows users to run VQE on their own machines if they wish.



(a) Original *Retrato de Mário de Andrade* by Anita Malfatti.

(b) Application of Chemical to Malfatti’s original piece.

Figure 10

3.3 Outcome

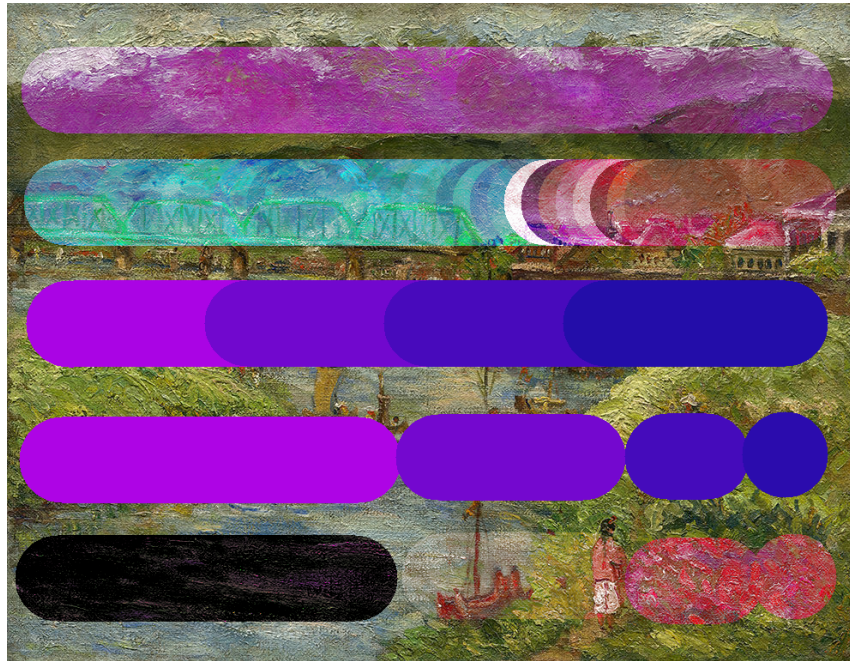
We apply Chemical to Anita Malfatti’s portrait of the Brazilian author Mário de Andrade [28] in Figure 10. The effect here is to highlight Anita’s strong blend of colors, smoothening the already remarkable mixture of colors in her work. A large radius was chosen, and different values for the bond distance were experimented. In the end, we opted for 0.735 \AA . We note that the disks generated by the averaging of HL values are clearly visible in the canvas. As mentioned in Section 3.2, although changing the number of repetitions usually mitigates this effect for monochromatic works, for a strong mixture of shades as Malfatti’s portrait, this is not usually the case, and the uniformization of the output strokes would ask for additional (classical) postprocessing.

In Figure 11a, it is possible to see the application of Chemical with different stroke thicknesses and bond distances to Tân Têng-pho’s *Taipei Bridge, Tamsui River* [10]. The distance parameter was set to 0.735 \AA for the three leftmost strokes, 1.6 \AA for the middle three strokes, and 2.5 \AA for the three right strokes. We see that, at least for H_2 , the smaller the bond distance, the more variety in the stroke colors, although it is hard to make this a general rule-of-thumb, as it might be a feature of the particular convergence rate of VQE only. Moreover, it is interesting to see that although the strokes start at the same state (top of the figure), modifying the distance seems to imply changing the estimated ground state, which is naturally expected given the Hamiltonian dependence on the average bond distances.

Figure 11b compares the effect of Chemical with the other stroke quantum brushes, namely Aquarela, Heisenbrush (continuous and discrete), and Smudge. Of these three, Aquarela is the most similar to Chemical, although its outcome is a significantly colder blend of colors. Once more, it is clear from the image that the original canvas’ underlying colors directly influence the brush’s outcome.



(a) Application of Chemical with different stroke thicknesses and bond distances to *Taipei Bridge, Tamsui River*.



(b) Brush effect comparison (from top to bottom): Aquarela, Chemical, Heisenbrush (continuous), Heisenbrush (discrete), and Smudge.

4 Conclusion

We presented two brushes based on variational methods, Steerable and Chemical, which we hope to incorporate within MOTH’s quantum brush kit. Some initial artistic uses of these brushes have been described in Sections 2.3 and 3.3, but we believe that much aesthetic value can be achieved by further exploring the tools. Nevertheless, there is still

plenty of room to improve on our current implementations, a task that we plan to address in the upcoming months.

Starting with Steerable, we would like to understand the exact reason for the decay of the colors towards gray when extrapolating, i.e., when t is set larger than 1. We believe that this behavior might be caused by either the particular choice of Hamiltonians in (6), but further experiments with different drifts and controls are necessary to clarify the process underlying this decay. Similarly, different learning strategies for u_1, \dots, u_n should be contrasted with our current technique. Of these, particularly interesting would be the incorporation of causality into the loss function, a method that has spawned interesting discussions in the specialized literature [13, 38]. In this same direction, it would be nice to contrast the results of the neural network method with other approximation algorithms, like GRAPE and CRAB. Finally, the use of GPU and early-stopping techniques for the training could significantly impact the user’s experience, but some care in operational system compatibility should be taken for their correct implementation.

For Chemical, we anticipate an expansion by including molecule options other than H_2 . Unfortunately, as elaborated in the main text, the current hyperparameters allow for only very slow convergence, which implies that the parametric lists of circuits $\{U(\boldsymbol{\eta}_j)\}_{j=1}^M$ soon become too big. To illustrate this point, we note that while VQE solutions of the H_2 ground state problem of 1000 different distances were computed in less than 8 minutes, computing solutions for the H_4 problem with only 50 distinct distances took approximately 7 hours. Once computed, the JSON file to store these H_4 solutions had 380 MB, versus 8 MB for storing H_2 ’s. This means that testing different combinations of hyperparameters is crucial for making other choices of molecules possible. Moreover, we would like to give the user the option to run VQE on their own and, potentially, to modify some of the hyperparameters—such as the basis and ordering of operators—to obtain different effects. Since our code for VQE depends on `qiskit-nature`, which has not been updated yet to work within `qiskit` 2’s framework [11], it is not trivial to run the algorithm without conflicting with the installation currently used by the other quantum brushes. We plan to work on an implementation independent from `qiskit-nature` to avoid this conflict until the package is updated by their developers.

References

- [1] Gabriele Agliardi, Dimitris Alevras, Vaibhaw Kumar, Roberto Lo Nardo, Gabriele Compostella, Sumit Kumar, Manuel Proissl, and Bimal Mehta. Portfolio construction using a sampling-based variational quantum scheme, 2025.
- [2] Francesca Albertini and Domenico D’Alessandro. Notions of controllability for bilinear multilevel quantum systems. *IEEE Transactions on Automatic Control*, 48(8):1399–1403, 2003.
- [3] Kishor Bharti, Alba Cervera-Lierta, Thi Ha Kyaw, Tobias Haug, Sumner Alperin-Lea, Abhinav Anand, Matthias Degroote, Hermanni Heimonen, Jakob S. Kottmann, Tim Menke, Wai-Keong Mok, Sukin Sim, Leong-Chuan Kwek, and Alán Aspuru-Guzik. Noisy intermediate-scale quantum algorithms. *Rev. Mod. Phys.*, 94:015004, Feb 2022.
- [4] Christopher M Bishop and Nasser M Nasrabadi. *Pattern recognition and machine learning*, volume 4. Springer, 2006.

- [5] Sergey Bravyi and Alexei Kitaev. Fermionic quantum computation. *Annals of Physics*, 298(1):210–226, 2002.
- [6] Constantin Brif, Raj Chakrabarti, and Herschel Rabitz. Control of quantum phenomena: past, present and future. *New Journal of Physics*, 12(7):075008, 2010.
- [7] Henrik Bruus and Karsten Flensberg. *Many-Body Quantum Theory in Condensed Matter Physics: An Introduction*. Oxford University Press, 2004.
- [8] Tommaso Caneva, Tommaso Calarco, and Simone Montangero. Chopped random-basis quantum optimization. *Physical Review A—Atomic, Molecular, and Optical Physics*, 84(2):022326, 2011.
- [9] Yu Cao, Shi Jin, and Nana Liu. Quantum neural ordinary and partial differential equations. *arXiv preprint arXiv:2508.18326*, 2025.
- [10] Chen Cheng-po. Taipei bridge, tamsui river. Oil on canvas, Ravenel International Art Group, 1933. Accessed via online catalogue: <https://ravenel.com/en/cata/lotsIn/d80a8943-0888-494d-b1ca-440b09f0d43c>.
- [11] qiskit-community/qiskit-nature community. “qiskit nature does not work with qiskit 2 (issue #1385)”. <https://github.com/qiskit-community/qiskit-nature/issues/1385>, 2025. Opened 6 Aug 2025.
- [12] Shantanu Debnath, Norbert M Linke, Caroline Figgatt, Kevin A Landsman, Kevin Wright, and Christopher Monroe. Demonstration of a small programmable quantum computer with atomic qubits. *Nature*, 536(7614):63–66, 2016.
- [13] Nathan Doumèche, Gérard Biau, and Claire Boyer. On the convergence of pinns. *Bernoulli*, 31(3):2127–2151, 2025.
- [14] Domenico d’Alessandro. *Introduction to quantum control and dynamics*. Chapman and hall/CRC, 2021.
- [15] Karin Erdmann and Mark J Wildon. *Introduction to Lie algebras*, volume 122. Springer, 2006.
- [16] Dmitry A Fedorov, Bo Peng, Niranjan Govind, and Yuri Alexeev. Vqe method: a short survey and recent developments. *Materials Theory*, 6(1):2, 2022.
- [17] João S. Ferreira, Arianna Crippa, Astryd Park, Daniel Bultrini, Pierre Fromholz, Roman Lipski, Karl Jansen, and James R. Wootton. Quantum brush: A quantum computing-based tool for digital painting, 2025.
- [18] Steffen J Glaser, Ugo Boscain, Tommaso Calarco, Christiane P Koch, Walter Köckenberger, Ronnie Kosloff, Ilya Kuprov, Burkhard Luy, Sophie Schirmer, Thomas Schulte-Herbrüggen, et al. Training schrödinger’s cat: Quantum optimal control: Strategic report on current status, visions and goals for research in europe. *The European Physical Journal D*, 69(12):279, 2015.
- [19] Harper R. Grimsley, Sophia E. Economou, Edwin Barnes, and Nicholas J. Mayhall. An adaptive variational algorithm for exact molecular simulations on a quantum computer. *Nature Communications*, 10(1):3007, 2019.

- [20] Brian C Hall. *Quantum theory for mathematicians*. Springer, 2013.
- [21] Trygve Helgaker, Poul Jørgensen, and Jeppe Olsen. *Molecular Electronic-Structure Theory*. John Wiley & Sons, 2000.
- [22] James E Humphreys. *Introduction to Lie algebras and representation theory*, volume 9. Springer Science & Business Media, 2012.
- [23] Paulo Vitor Itaboraí, Tim Schwägerl, María Aguado Yáñez, Arianna Crippa, Karl Jansen, Eduardo Reck Miranda, and Peter Thomas. Variational quantum harmonizer: Generating chord progressions and other sonification methods with the vqe algorithm. *arXiv preprint arXiv:2309.12254*, 2023.
- [24] Pascual Jordan and Eugene Wigner. Über das paulische äquivalenzverbot. *Zeitschrift für Physik*, 47:631–651, 1928.
- [25] Navin Khaneja, Timo Reiss, Cindie Kehlet, Thomas Schulte-Herbrüggen, and Stefan J Glaser. Optimal control of coupled spin dynamics: design of nmr pulse sequences by gradient ascent algorithms. *Journal of magnetic resonance*, 172(2):296–305, 2005.
- [26] Alexander A Kirillov. *An introduction to Lie groups and Lie algebras*, volume 113. Cambridge University Press, 2008.
- [27] Masatake Kuranishi. On everywhere dense imbedding of free groups in lie groups. *Nagoya Mathematical Journal*, 2:63–71, 1951.
- [28] Anita Malfatti. Portrait of mário de andrade i. Painting, 1921–22. Oil on canvas, 51 × 41 cm; private collection, São Paulo.
- [29] Eduardo Reck Miranda. *Advances in Quantum Computer Music*. WORLD SCIENTIFIC, August 2024.
- [30] Joan Miró. El jardín / the garden. Painting, 1925. Oil on canvas, ca. 86 × 71 cm.
- [31] Alberto Peruzzo, Jarrod McClean, Peter Shadbolt, Man-Hong Yung, Xiao-Qi Zhou, Peter J Love, Alán Aspuru-Guzik, and Jeremy L O'brien. A variational eigenvalue solver on a photonic quantum processor. *Nature communications*, 5(1):4213, 2014.
- [32] IBM Quantum. The variational quantum eigensolver (vqe). Online course module, 2025. Accessed: 2025-11-17.
- [33] Viswanath Ramakrishna, Murti V Salapaka, Mohammed Dahleh, Herschel Rabitz, and Anthony Peirce. Controllability of molecular systems. *Physical Review A*, 51(2):960, 1995.
- [34] Pierre-Auguste Renoir. Bal du moulin de la galette. Oil on canvas, 1876. Musée d'Orsay, Paris.
- [35] Isaac D Smith, Maxime Cautrès, David T Stephen, and Hendrik Poulsen Nautrup. Optimally generating $\text{su}(2^n)$ using pauli strings. *Physical Review Letters*, 134(20):200601, 2025.
- [36] Attila Szabo and Neil S. Ostlund. *Modern Quantum Chemistry: Introduction to Advanced Electronic Structure Theory*. Dover Publications, 1996.

- [37] Gabriel Turinici. On the controllability of bilinear quantum systems. In *Mathematical models and methods for ab initio Quantum Chemistry*, pages 75–92. Springer, 2000.
- [38] Sifan Wang, Shyam Sankaran, and Paris Perdikaris. Respecting causality for training physics-informed neural networks. *Computer Methods in Applied Mechanics and Engineering*, 421:116813, 2024.
- [39] Andy Warhol. Marilyn diptych. Synthetic polymer paint and silkscreen ink on canvas, 1962. Diptych, Tate Modern, London.

A Quantum Chemistry

In this appendix, we detail the quantum-chemical formalism underlying the Chemical brush. To avoid redundancy, we assume that the reader is familiar with the variational principle and with the VQE workflow already described in 3.1. Unless otherwise explicit, this whole section is based on [21, 36].

We recall that the goal is to compute the ground electronic energy of a molecule. We tackle this by solving the eigenvalue problem for the Born–Oppenheimer electronic Hamiltonian, \hat{H} , in the antisymmetric N -electron sector. In practice, we project the problem to a finite Galerkin subspace $\mathcal{H}_{N,M}$ spanned by chosen spin–orbitals, which turns \hat{H} into a finite Hermitian matrix whose eigenvalues are the electronic energy levels. This matrix is mapped to qubits (Jordan–Wigner or Bravyi–Kitaev) Jordan–Wigner [24] or Bravyi–Kitaev [5] as a Pauli sum so that we can build an associated parametrized quantum circuit whose parameters are minimized variationally with VQE using either a chemistry-inspired DUCC (UCCSD pool or ADAPT-selected) [19] or a hardware-efficient $SU(2)$ ansatz. Expectations are measured on hardware (leveraging quantum), and parameters are updated classically in the hope of eventually getting the smallest eigenvalue and its associated eigenvector representing the energy of the system as described in Section 3. In practice, most of these steps can be undertaken automatically with `qiskit` and `qiskit-nature`.

Space of particles. We start by considering a system of one particle only. Let $\mathfrak{h} = L^2(\mathbb{R}^3) \otimes \mathbb{C}^2$ denote the Hilbert space of a single electron (square-integrable spatial wavefunctions times spin- $\frac{1}{2}$). For simple tensors, $\langle \phi \otimes \sigma, \psi \otimes \tau \rangle_{\mathfrak{h}} = \langle \phi, \psi \rangle_{L^2} \langle \sigma, \tau \rangle_{\mathbb{C}^2}$, extended sesquilinearly. We define the Fock space and N -electron sector

$$\mathcal{F} = \bigoplus_{N=0}^{\infty} \wedge^N \mathfrak{h},$$

with $\wedge^N \mathfrak{h}$ the antisymmetric wedge product. For a fixed electron number N (hence, a fixed number of atoms), the physical Hilbert space considered is the antisymmetric sector

$$\mathcal{H}_N = \wedge^N \mathfrak{h} \subset \mathcal{F}.$$

Given the fixed N -electron Hilbert space $\mathcal{H}_{N,M} = \wedge^N \mathfrak{h}_M$, the next step is to introduce a representation of operators that act on this space under fermionic statistics, for example, all many-electron operators are expressed in terms of creation and annihilation operators that satisfy the canonical anticommutation relation (CAR) [7]. These operators encode

the Pauli exclusion principle and provide an algebraic basis from which any observable on $\mathcal{H}_{N,M}$ can be constructed.

We can use this to define the creation and annihilation operators. Explicitly, for $f \in \mathfrak{h}$, define $a^\dagger(f), a(f) : \mathcal{F} \rightarrow \mathcal{F}$ by

$$a^\dagger(f)(\psi_1 \wedge \cdots \wedge \psi_N) = f \wedge \psi_1 \wedge \cdots \wedge \psi_N, \quad a(f) = (a^\dagger(f))^*,$$

satisfying the canonical anticommutation relations (CAR)

$$\{a(f), a(g)\} = 0, \quad \{a^\dagger(f), a^\dagger(g)\} = 0, \quad \{a(f), a^\dagger(g)\} = \langle f, g \rangle_{\mathfrak{h}} \text{Id}_{\mathcal{F}}.$$

If $(\chi_p)_{p \geq 1}$ is an orthonormal system in \mathfrak{h} , then $a_p^\dagger = a^\dagger(\chi_p)$, $a_p = a(\chi_p)$ obey $\{a_p, a_q\} = 0$, $\{a_p^\dagger, a_q^\dagger\} = 0$, $\{a_p, a_q^\dagger\} = \delta_{pq}$.

Born–Oppenheimer electronic Hamiltonian. Having fixed the state space and the algebra of fermionic operators acting on it, the next ingredient is the electronic Hamiltonian associated with clamped nuclei. With nuclear positions (\mathbf{R}_A) and charges (Z_A) held fixed, the nonrelativistic electronic Hamiltonian is the self-adjoint operator

$$\hat{H} = \sum_{k=1}^N \left(-\frac{1}{2} \Delta_{\mathbf{r}_k} - \sum_A \frac{Z_A}{|\mathbf{r}_k - \mathbf{R}_A|} \right) + \sum_{1 \leq k < \ell \leq N} \frac{1}{|\mathbf{r}_k - \mathbf{r}_\ell|},$$

acting on \mathcal{H}_N . Its eigenvalues are real and correspond to electronic energy levels. The eigenvalue problem $\hat{H} |\phi_k\rangle = E_k |\phi_k\rangle$ is therefore the mathematical formulation of the calculation of the ground-state energy.

To make the problem computationally tractable, we choose M orthonormal spin-orbitals $\{\chi_p\}_{p=1}^M \subset \mathfrak{h}$ (constructed from a Gaussian basis and spin functions) and restrict the model to the truncated Galerkin subspace

$$\mathcal{H}_{N,M} = \wedge^N \mathfrak{h}_M, \quad \dim \mathcal{H}_{N,M} = \binom{M}{N},$$

where $\mathfrak{h}_M = \text{span}\{\chi_p\} \cong \mathbb{C}^M$. All operators considered below are the projections of their full-space counterparts onto $\mathcal{H}_{N,M}$, where they admit finite Hermitian matrix representations.

Second quantization on $\mathcal{H}_{N,M}$. In the chosen orbital basis, the Hamiltonian coefficients are the standard one- and two-electron integrals,

$$\begin{aligned} h_{pq} &= \int \chi_p^*(\mathbf{r}) \left(-\frac{1}{2} \nabla^2 - \sum_A \frac{Z_A}{|\mathbf{r} - \mathbf{R}_A|} \right) \chi_q(\mathbf{r}) d\mathbf{r} \\ v_{pqrs} &= \iint \frac{\chi_p^*(\mathbf{r}_1) \chi_q^*(\mathbf{r}_2) \chi_r(\mathbf{r}_1) \chi_s(\mathbf{r}_2)}{|\mathbf{r}_1 - \mathbf{r}_2|} d\mathbf{r}_1 d\mathbf{r}_2, \end{aligned}$$

leading to the compact operator expression

$$\hat{H} = \sum_{p,q=1}^M h_{pq} a_p^\dagger a_q + \frac{1}{2} \sum_{p,q,r,s=1}^M v_{pqrs} a_p^\dagger a_q^\dagger a_s a_r.$$

For any occupation pattern $\text{Occ} \subset \{1, \dots, M\}$ with $|\text{Occ}| = N$, the Slater determinant

$$|\Phi_{\text{Occ}}\rangle = \bigwedge_{i \in \text{Occ}} \chi_i = \prod_{i \in \text{Occ}} a_i^\dagger |0\rangle$$

forms part of an orthonormal basis of $\mathcal{H}_{N,M}$. The matrix elements of \hat{H} on this basis follow the Slater–Condon rules: they vanish unless determinants differ by at most two spin-orbitals; the nonzero elements involve h_{pq} and antisymmetrized v_{pqrs} . The Hartree–Fock determinant $|\Phi_{\text{HF}}\rangle$ serves as the reference configuration.

Fermion-to-qubit encodings. To evaluate expectation values on qubit hardware, the fermionic mode operators (creation and annihilation) are mapped to Pauli strings. For example, the Jordan–Wigner transform gives [24]

$$a_p^\dagger = \frac{1}{2}(X_p - iY_p) \bigotimes_{j=1}^{p-1} Z_j, \quad a_p = \frac{1}{2}(X_p + iY_p) \bigotimes_{j=1}^{p-1} Z_j,$$

so that

$$\hat{H} = \sum_{\alpha=1}^T c_\alpha P_\alpha, \quad P_\alpha \in \{I, X, Y, Z\}^{\otimes M}, \quad c_\alpha \in \mathbb{R},$$

with T polynomial in M after exploiting symmetries and tapering.

VQE terminology and cost functional. Given a parametrized ansatz $|\psi(\boldsymbol{\eta})\rangle = U(\boldsymbol{\eta})|\Phi_{\text{HF}}\rangle$, the variational energy evaluated on qubits is

$$E(\boldsymbol{\eta}) = \sum_{\alpha} c_\alpha \langle \psi(\boldsymbol{\eta}) | P_\alpha | \psi(\boldsymbol{\eta}) \rangle.$$

A VQE iteration alternates between estimating these Pauli expectations on hardware and updating $\boldsymbol{\eta}$ via classical optimization.

Ansätze used (DUCC and hardware-efficient $SU(2)$). Let τ_μ denote fermionic excitation operators relative to $|\Phi_{\text{HF}}\rangle$ and $\kappa_\mu = \tau_\mu - \tau_\mu^\dagger$.

- **Disentangled UCC (DUCC).** A product ansatz of the form

$$U_{\text{DUCC}}(\mathbf{t}) = \prod_{\mu \in \mathcal{A}} \exp(t_\mu \kappa_\mu),$$

where \mathcal{A} is a pool of spin-preserving singles and doubles (UCCSD) or an adaptive ADAPT-selected set [19].

- **Hardware-efficient $SU(2)$.** A layered structure

$$U_{\text{SU}(2)}(\boldsymbol{\eta}) = \prod_{\ell=1}^L \left(\bigotimes_{q=1}^n R_y(\eta_{\ell,q}) R_z(\phi_{\ell,q}) \right) \prod_{\ell=1}^{L-1} \text{Entangle}_\ell,$$

using fixed entangling patterns (CZ/CNOT).

Note that all brush simulations operate entirely within $\mathcal{H}_{N,M}$, so \hat{H} is represented exactly as a finite Hermitian matrix and its qubit encoding uses a finite Pauli expansion.

Quantity	Value
Fock-space dimension	$\binom{4}{2} = 6$
Determinants (HF first)	1100, 1010, 1001, 0110, 0101, 0011
Reference index	0
Singles	(0, 1), (0, 2), (0, 3), (0, 4)
Doubles	(0, 5)
Total DUCC excitations	5
α orbitals	[0, 2]
β orbitals	[1, 3]
Spin-pres. singles	(0, 2), (1, 3)
Spin-pres. doubles	((0, 1), (2, 3))
Total spin-pres. excitations	3

Table 2: DUCC excitation structure for H₂ in STO–3G.

Excitation set, Ordering effects, and Practical Choices The construction above fixes the Hilbert space, operator algebra, and truncation. We now instantiate these objects in an explicit orbital basis and record the coefficients entering the second-quantized Hamiltonian.

A central modelling choice for the Unitary Coupled Cluster Ansatz (UCC) is the set of operators to consider and their ordering of unitaries that are not commutative. Although the exact ground state lies in the full configuration interaction (FCI) space, the variational trajectory obtained on hardware depends on three structural parameters: the excitation pool used, the ordering of the excitation operators in the disentangled DUCC product, and the molecular data defining the active space (basis, interatomic geometry, and spin structure).

To illustrate how the active-space structure determines the excitation set, we record the DUCC excitation spaces for H₂ in minimal bases.

Example: H₂ in STO–3G

For $n_{\text{orb}} = 4$ spin-orbitals and $n_{\text{elec}} = 2$ electrons, the truncated Fock space has dimension $\binom{4}{2} = 6$. Table 2 summarizes the determinant ordering, the DUCC excitation manifold, and the corresponding spin-preserving operators used by `qiskit` conventions.

This structure completely characterizes the disentangled UCCSD ansatz used by the Brush for H₂ in the minimal basis.